

Lessons learnt from synergistic use of polar and geostationary satellite sensors for the retrieval of aerosol characteristics

Maria João Costa^{a,b}, Marco Cervino^a, Elsa Cattani^a, Francesca Torricella^a, Vincenzo Levizzani^a, and Ana Maria Silva^b

^aInstitute of Atmospheric and Oceanic Sciences (ISAO-CNR), Via Gobetti 101, Bologna I-40129, Italy

^bUniversity of Évora, Department of Physics, Rua Romão Ramalho 59, 7000 Évora, Portugal

ABSTRACT

The interest in aerosol observations from satellite passive instrument is steadily increasing since satellite instruments supply unique global observations for establishing an aerosol climatology. A correct characterization of single aerosol events from satellite requires adequate temporal and spatial resolution. Most state-of-the-art algorithms are based on a single sensor, so that they often suffer from specific limitations: poor spatial or spectral resolution, large re-visitation time, poor de-clouding,...

A method to exploit the synergy between the polar orbiting instrument GOME (Global Ozone Monitoring Experiment) and the METEOSAT geostationary system was proposed¹, aiming at increasing the accuracy of the aerosol characterization over the ocean by determining with GOME the actual aerosol model to be adopted for aerosol optical thickness determination with METEOSAT.

Applications of the algorithm to relevant aerosol events are presented characterizing aerosol optical properties and thickness. The comparison with results obtained via independent space-time co-located ground-based measurements and retrievals from other algorithms that make use of satellite measurements such as POLDER, allows for a first validation of the algorithm. Comparisons also address limitations of the retrieved aerosol model in terms of time-space coverage.

Keywords: aerosol, satellite, synergy, validation

1. INTRODUCTION

Aerosol particles play a major role in the atmospheric processes. Particles scatter and absorb solar radiation and enter cloud microphysical processes as cloud condensation nuclei, heavily affecting precipitation processes, as recently confirmed^{2,3}.

Since these effects can be extremely relevant, not only an accurate characterization of aerosol particles is essential, but also a monitoring of their evolution in terms of load (aerosol optical thickness) and type. This can be achieved using measurements from satellite sensors. However, an accurate monitoring of aerosols can be problematic if a single sensor strategy is adopted, since presently there is no satellite with optimum spatial/temporal/spectral resolution and coverage. Geostationary satellites assure adequate spatial and, most important, temporal resolution for monitoring the aerosol optical thickness on the global scale^{4,5}. However, because of lack of spectral resolution needed to characterize aerosol properties, aerosol retrieval techniques are constrained to use fixed aerosol classes based on climatology. This can introduce considerable errors on aerosol optical thickness retrievals, since classes refer to mean atmospheric conditions that may not represent the actual state of the atmosphere. Note that sensors onboard polar satellites are not appropriate to monitor atmospheric aerosol concentrations due to their poor temporal resolution. Nevertheless, some of these sensors supply essential data for an accurate aerosol analysis and characterization. In particular the GOME spectrometer⁶ onboard the polar

For further author information -

mjcosta@uevora.pt; phone +39 051 6399579; fax +39 051 6399649; m.cervino@isao.bo.cnr.it; phone +39 051 6399579; fax +39 051 6399649; e.cattani@isao.bo.cnr.it; phone +39 051 6399578; fax +39 051 6399649; f.torricella@isao.bo.cnr.it; phone +39 051 6399580; fax +39 051 6399649; v.levizzani@isao.bo.cnr.it; phone +39 051 6399578; fax +39 051 6399649; asilva@uevora.pt; phone +351 266 744616; fax +351 266 702306

<http://www.isao.bo.cnr.it/~meteosat/>; <http://www.dfis.uevora.pt>

orbiting satellite ERS-2 (European Remote Sensing Satellite) is successfully used to retrieve aerosol properties over the ocean^{7, 8}. Despite its low spatial resolution, the techniques take advantage of its high spectral resolution to avoid gas absorption as much as possible.

The present work tries to overcome the obvious limitations that measurements from geostationary as well as polar platforms present, aiming at extending the accurate aerosol characterization obtained from polar sensors to the geostationary scale, which assure adequate spatial and temporal resolution for monitoring purposes¹.

Available results demonstrate the potential of the method for a possible contribution to a long term aerosol accurate global monitoring and climatology. This conclusion can be drawn from comparisons with totally independent results as the aerosol optical properties and thickness obtained from the ground-based sun/sky-photometer network AERONET (AERosol RObotic NETwork) and the aerosol optical thickness from the POLDER (POLARization and Directionality of Earth Reflectances) algorithm⁹.

In the following sections the algorithm is described and aerosol properties results and validation are presented and discussed for several desert dust transports that occurred over the Atlantic Ocean during June and July 1997.

2. METHODOLOGY AND RESULTS

The method can be divided in three main steps that are described next. Firstly the selection of homogeneous GOME pixels over the ocean that provide valuable spectral information for aerosol characterization; secondly the fitting of the GOME measured selected spectra with simulated spectra, thus retrieving the effective aerosol optical properties and finally the use of these properties in combination with METEOSAT broad band visible measurements for aerosol optical thickness retrieval, avoiding literature aerosol classes based on climatology.

2.1 Automated GOME spectral measurement selection

The retrieval of aerosol properties from GOME spectral measurements requires a preparatory spectral and geographical pixel selection where aerosol particles are to be modeled with fewer uncertainties.

GOME measures the Earthshine radiance and solar irradiance in the spectral range between 0.240 and 0.793 μm , with high spectral resolution that varies between 0.2×10^{-3} and $0.4 \times 10^{-3} \mu\text{m}$. It is thus possible to choose spectral regions where gas absorption is kept to a minimum; the four wavelengths selected for the retrievals are 0.361, 0.421, 0.753 and 0.783 μm .

Geographical areas (pixels) selected to perform the inversions should correspond exclusively to cloud free areas over the ocean, with low reflectance variability that ensures pixel homogeneity. This selection is problematic due to the lack of GOME spectral information in the infrared spectral region for cloud detection as well as to the dimension of GOME pixels ($320 \times 40 \text{ Km}^2$). This is overcome using GOME and METEOSAT blended data: GOME geo-location is matched with METEOSAT best time coincident classified images (maximum time difference is 15 minutes; often better). METEOSAT classification is based on a statistical VIS-IR algorithm¹⁰ developed for METEOSAT channels. It allows for the distinction of several classes, namely clouds,

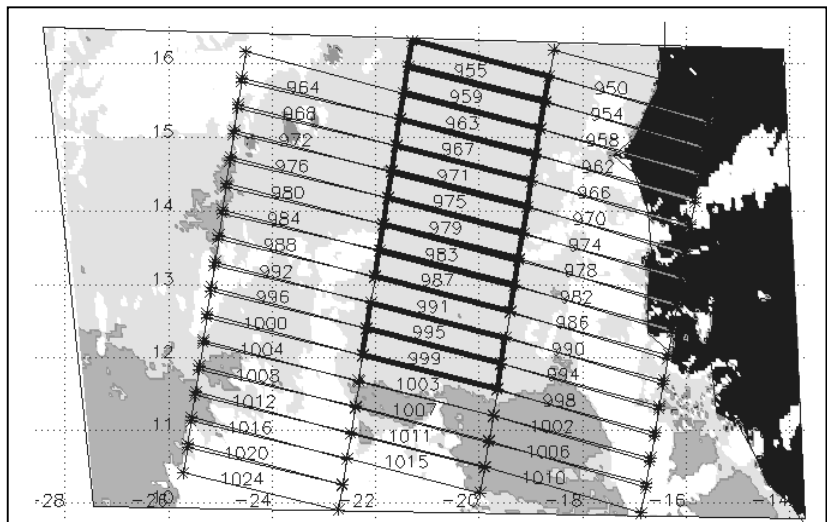


Figure 1: Example of GOME pixel selection for 3 June 1997. The figure represents a classified cut image of the METEOSAT-6 full disk image (slot 25) and overlapped the GOME pixel geo-location. Classes represented are: land (black), clouds (white), background aerosol – water (whitish) and strong aerosol contamination (gray). GOME pixels bounded with the thick line are considered homogeneous and represent the selections for this scene.

land, water and strong aerosol contamination, at spatial resolution of $5 \times 5 \text{ Km}^2$ at the sub-satellite point. The different spatial resolution between the two sensors (METEOSAT and GOME) is taken into account when overlapping both geolocations by determining which METEOSAT pixels are located inside each GOME pixel. The latter is selected for the inversion only if the METEOSAT pixels that fall inside it are all classified as water or all classified as aerosol contaminated, thus ensuring spatial homogeneity inside the pixel. 209 GOME pixels are selected from the orbits analyzed for June 1997. Figure 1 shows an example of the selection.

2.2 Aerosol optical properties retrieval from GOME

Once METEOSAT data has been used to select adequate GOME pixels, aerosol microphysical parameters may be retrieved by fitting the GOME spectral reflectance measurements with simulated spectral reflectance, varying some of the parameters characterizing aerosols.

Simulations are done with the radiative transfer model 6S (Second Simulation of the Satellite Signal in the Solar Spectrum¹¹). The ocean surface is considered as a lambertian reflector and a tropical atmospheric vertical profile is taken. The impact of using such approximations has already been addressed¹².

Mode	Modal radius (μm)	Standard Deviation of the mod. radius (μm)	Percentage number density of particles
Fine	0.01-1.0	0.398	99.9
Coarse	0.5-10.0	0.301	0.1

Table 1: Size distribution parameters. Identified in bold the lower and upper variation limits of the fitting parameters.

Aerosol characterization assumes a bimodal lognormal size distribution with a fine and a coarse mode, and a common spectral complex refractive index for both modes. The modal radii of the size distribution, the imaginary part of the refractive index in two spectral regions and the aerosol optical thickness are the free (within established limits - see tables 1 and 2) fitting parameters. The spectral regions considered for imaginary refractive index retrievals, are $0.35 - 0.50 \mu\text{m}$ and $0.70 - 0.86 \mu\text{m}$. The aerosol type class

(maritime or desert) is chosen accordingly to the aforementioned METEOSAT classification.

The mathematical method used to fit the simulated spectra to the measurements is the continuous minimization by simulated annealing¹³. This is a well-suited method for finding the global minimum of a function in the presence of several local minima. It is applied to the minimization of the chi-square function, which describes the agreement between measurements and simulations.

Aerosol Type class	Spectral Complex Refractive Index	
	Spectral regions (μm)	
	0.35 - 0.50	0.70 - 0.86
Maritime	1.40 - (0.0 - 0.05) i	1.40 - (0.0 - 0.01) i
Desert	1.48 - (0.0 - 0.05) i	1.48 - (0.0 - 0.01) i

Table 2: Complex refractive index parameters for a maritime and desert type aerosol classes. Identified in bold the lower and upper variation limits of the fitting parameters.

The present algorithm is composed by two distinct minimizations. The first one varies the size distribution modal radii and the spectral imaginary refractive indexes. In the second one only the aerosol optical thickness is varied from its initially fixed value⁸; the parameters obtained from the first fitting remain unchanged, in order to adjust the aerosol optical thickness to the new microphysical properties. The functions chi-square to be minimized in the two are:

$$\chi^2(R_F, R_C, \text{Im}_1, \text{Im}_2) = \sum_{i=1}^n \left(\frac{\rho^G(\lambda_i) - \rho^S(\lambda_i, \tau_a^*; R_F, R_C, \text{Im}_1, \text{Im}_2)}{\sigma(\lambda_i)} \right)^2 \quad (1)$$

$$\chi^2(\tau_a) = \sum_{i=1}^n \left(\frac{\rho^G(\lambda_i) - \rho^S(\lambda_i; \tau_a)}{\sigma(\lambda_i)} \right)^2 \quad (2)$$

where τ_a^* is the aerosol optical thickness initialization value, R_F and R_C the modal radii of the fine and coarse mode, respectively, Im_1 and Im_2 the imaginary parts of the refractive index for the two chosen spectral regions, and τ_a the retrieved

aerosol optical thickness. $\rho^G(\lambda_i)$ and $\rho^S(\lambda_i)$ are the measured and simulated GOME spectral reflectance, respectively, $\sigma(\lambda_i)$ the standard deviations associated with GOME spectral measurements and n the number of selected wavelengths λ_i .

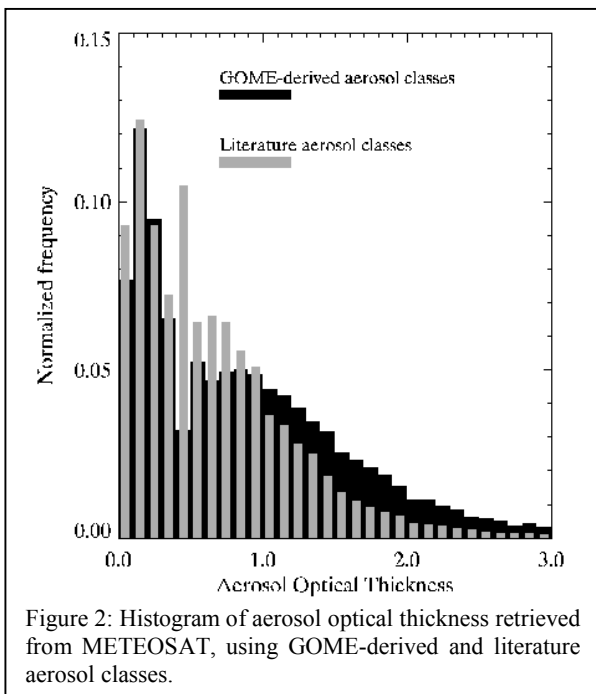
The parameters obtained from the fitting are analyzed in order to obtain effective aerosol classes describing the actual atmospheric conditions, substitutive of literature classes. A problem is identifying the limit between maritime or desert type aerosols. The criterion adopted uses the value of the aerosol optical thickness obtained from the second fitting, with a discriminating value of 0.4. This threshold stems from the analysis of the aerosol optical thickness and imaginary refractive index results obtained from GOME spectral measurement fitting for the selected pixels. There is a significant increase in the imaginary part of the refractive index (0.35 - 0.50 μm) for optical thicknesses around 0.4, which suggests a substantial increase in aerosol absorption and consequently a different type of aerosol (desert).

Aerosol Type class	Mode	Modal radius (μm)	Standard Deviation of the mod. radius (μm)	Percentage number density of particles	Spectral Complex Refractive Index	
					Spectral regions (μm)	
					0.35 – 0.50	0.70 – 0.86
Maritime	Fine	0.23	0.398	99.9	1.40 – 0.000643i	1.40 – 0.0000866i
	Coarse	2.58	0.301	0.1		
Desert	Fine	0.14	0.398	99.9	1.48 – 0.0032i	1.48 – 0.0012i
	Coarse	3.07	0.301	0.1		

Table 3: Mean size distributions and complex refractive indexes retrieved from the selected GOME spectral reflectance inversion. Mean retrieved parameters are presented in bold.

From the 209 selected pixels, 60% of the results are used to derive the maritime type class and the remaining 40% for the desert class. Two GOME-derived aerosol classes are then defined, one typical of clear maritime conditions and another of desert dust events (parameters are summarized in table 3). Although data belong to the whole June, pixels with the required conditions refer mainly to the first half of the month, especially for the desert class where 94% of the data is from the first half of June.

The optical parameters are obtained assuming spherical aerosol particles, hence applying Mie theory to the GOME-derived aerosol microphysics.



2.3 Aerosol optical thickness retrieval from METEOSAT

The aim is now to succeed in extending the aerosol optical thickness retrievals to the geostationary time and space scales. Aerosol optical properties derived from GOME spectral measurement fitting are thus combined with METEOSAT data to retrieve the aerosol optical thickness, using actual aerosol properties instead of literature classes, aiming at more accurate retrievals.

The aerosol optical thickness is calculated using METEOSAT-6 visible measurements averaged 2x2 from the original full resolution disk image, leading to a pixel resolution of 5x5 Km² at nadir. For this purpose Lookup Tables (LUTs) of METEOSAT-6 visible radiances are built for 9 values of the optical thickness (0.0, 0.1, 0.2, 0.5, 1.0, 1.5, 2.0, 2.5, 3.0) and for the two aerosol classes derived from GOME spectral measurement fitting (maritime and desert type). Geometry is taken into account building the LUTs with 2° resolution in solar and satellite zenith angles.

The geographical area is enclosed in a latitude box between 10° and 30° N and longitude between 10° and 50° W. In this area the

occurrence of strong Saharan dust events is very common, especially during the northern hemisphere summer. This is due to the almost complete absence of rain during this season, which prevents the deposition of dust particles and allows their long distance transport. In fact at least one strong dust outbreak occurred during June 1997, the period selected for the study.

Aerosol optical thickness is also retrieved using maritime and desert aerosol classes available in the literature^{11, 14}, in order to compare them with results obtained from the new aerosol classes and verify their impact in the accuracy of retrievals.

Figure 2 shows the histogram of the aerosol optical thickness retrieved from METEOSAT-6 measurements, for the GOME-derived and the literature aerosol classes. It represents about 5 million METEOSAT pixels processed during June 1997. Clearly when using GOME-derived aerosol classes, a bimodal distribution of the aerosol optical thickness can be distinguished, correspondent to a background maritime situation superimposed to a strong Saharan dust transport event. The same is obtained when literature aerosol classes are used. Whilst the modes correspondent to the background maritime occurrences (low optical thickness values) are very similar, substantial differences can be noted for optical thickness values related to dust events. Moreover, the systematic difference in optical thickness arising from the use of the different aerosol classes for the desert transport situation increases with the optical thickness. This shows the significant impact of choosing different aerosol classes, especially for strong aerosol events. The importance of retrieving the actual aerosol class from GOME spectral measurements is shown in the next section, dedicated to the validation.

3. VALIDATION

3.1 Aerosol optical properties retrieved from GOME

Aerosol optical properties derived from GOME spectral measurement fitting are compared with those derived from the AERONET at selected locations¹⁵. This latter derives simultaneously the aerosol size distribution, complex refractive index and single scattering albedo, from spectral measurements of direct and diffuse radiation, obtained with the Sun-sky scanning radiometers of AERONET.

Results from the Dakar site during June and July 1997 are analyzed in order to calculate aerosol optical properties characteristic of desert dust aerosols, using Mie theory. The site is in fact over passed by dust plumes several times. The mean properties for the selected periods over the site are obtained retaining only the cases where the solar zenith angle is greater than 45° and aerosol optical thickness at 0.44 μm greater than 0.5¹⁶. The latter conditions are imposed to determine the actual desert aerosol characteristics. Figures 3 and 4 show comparisons between a literature aerosol desert model¹⁴, the GOME-derived aerosol properties for June 1997, and the two AERONET-derived desert aerosol optical properties (Dakar – June and July).

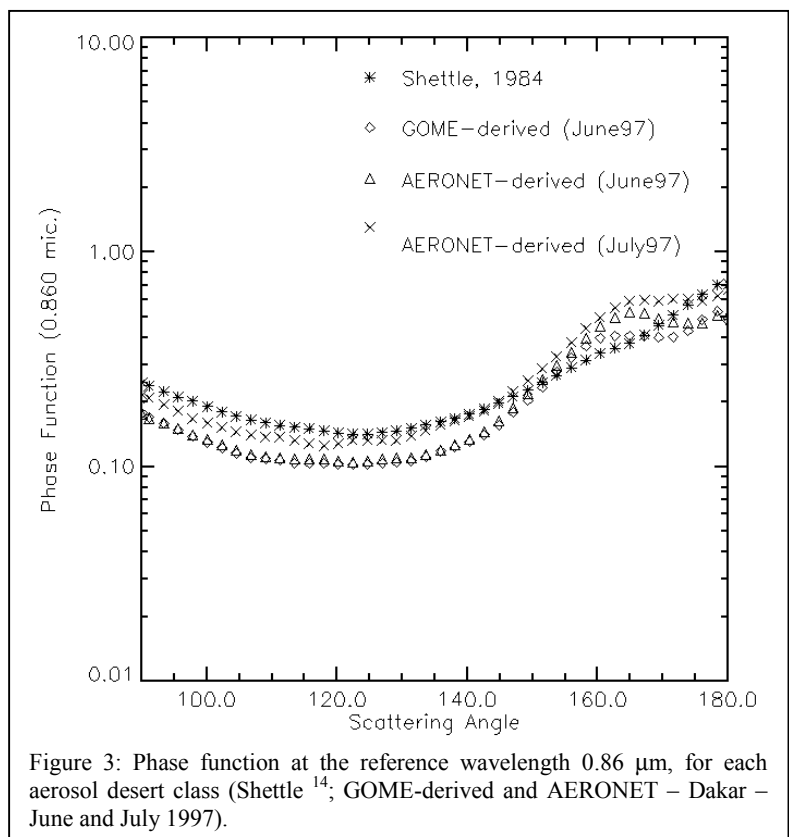


Figure 3: Phase function at the reference wavelength 0.86 μm, for each aerosol desert class (Shettle¹⁴; GOME-derived and AERONET – Dakar – June and July 1997).

The aerosol class obtained from the fitting of GOME spectral measurements is almost entirely in good agreement with the actual aerosol optical properties represented by the AERONET results (June 1997). In fact, the agreement of the spectral asymmetry parameter and phase function derived from GOME with AERONET results is excellent. More relevant discrepancies are obtained for the scattering coefficient, although even in this case the agreement is better for the GOME-derived class than for the literature one.

Monthly mean aerosol optical properties measured in Dakar during July 1997 present some differences with respect to both AERONET and GOME-derived properties for the previous month. This hints to the fact that the effective class retrieved from the fitting of GOME spectra does not effectively represent the mean actual aerosol characteristics during July, as it does for June. The literature class does not reproduce the actual aerosol characteristics in any of the analyzed cases.

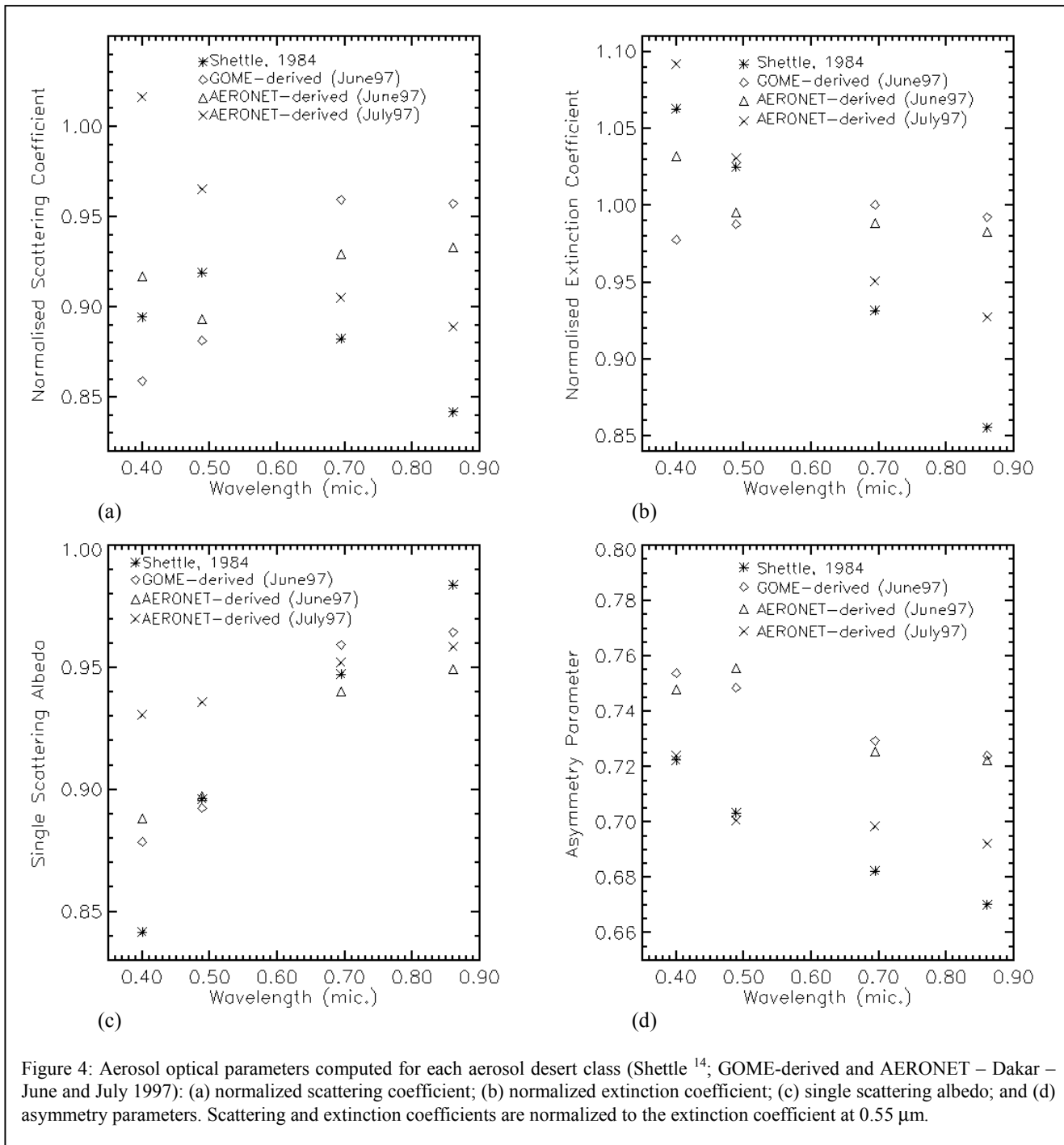


Figure 4: Aerosol optical parameters computed for each aerosol desert class (Shettle ¹⁴, GOME-derived and AERONET – Dakar – June and July 1997): (a) normalized scattering coefficient; (b) normalized extinction coefficient; (c) single scattering albedo; and (d) asymmetry parameters. Scattering and extinction coefficients are normalized to the extinction coefficient at 0.55 μm .

3.2 Aerosol optical thickness retrieved from METEOSAT

Four AERONET stations are selected for aerosol optical thickness validation, namely Dakar (14.394°N, 16.959°W), Cabo Verde (16.733°N, 22.935°W), Tenerife (28.033°N, 16.633°W) and Izana (28.300°N, 16.500°W). For the comparisons, METEOSAT pixel radiances enclosed in a box of 0.5°x0.5° centered on the geographical location of the ground-based station are spatially averaged and the respective standard deviations computed, discarding all cloud-land contaminated pixels. Aerosol optical thickness values from AERONET stations are taken within about fifteen minutes from the METEOSAT scan over the area. Values are time averaged and the standard deviation over the half-hour period is computed. AERONET averaged optical thickness is taken for the comparisons only if the correspondent standard deviation is lower than 0.2. As for the spatially averaged optical thickness derived from METEOSAT, values greater than 1.0 are taken only if the correspondent standard deviation is lower than 0.5.

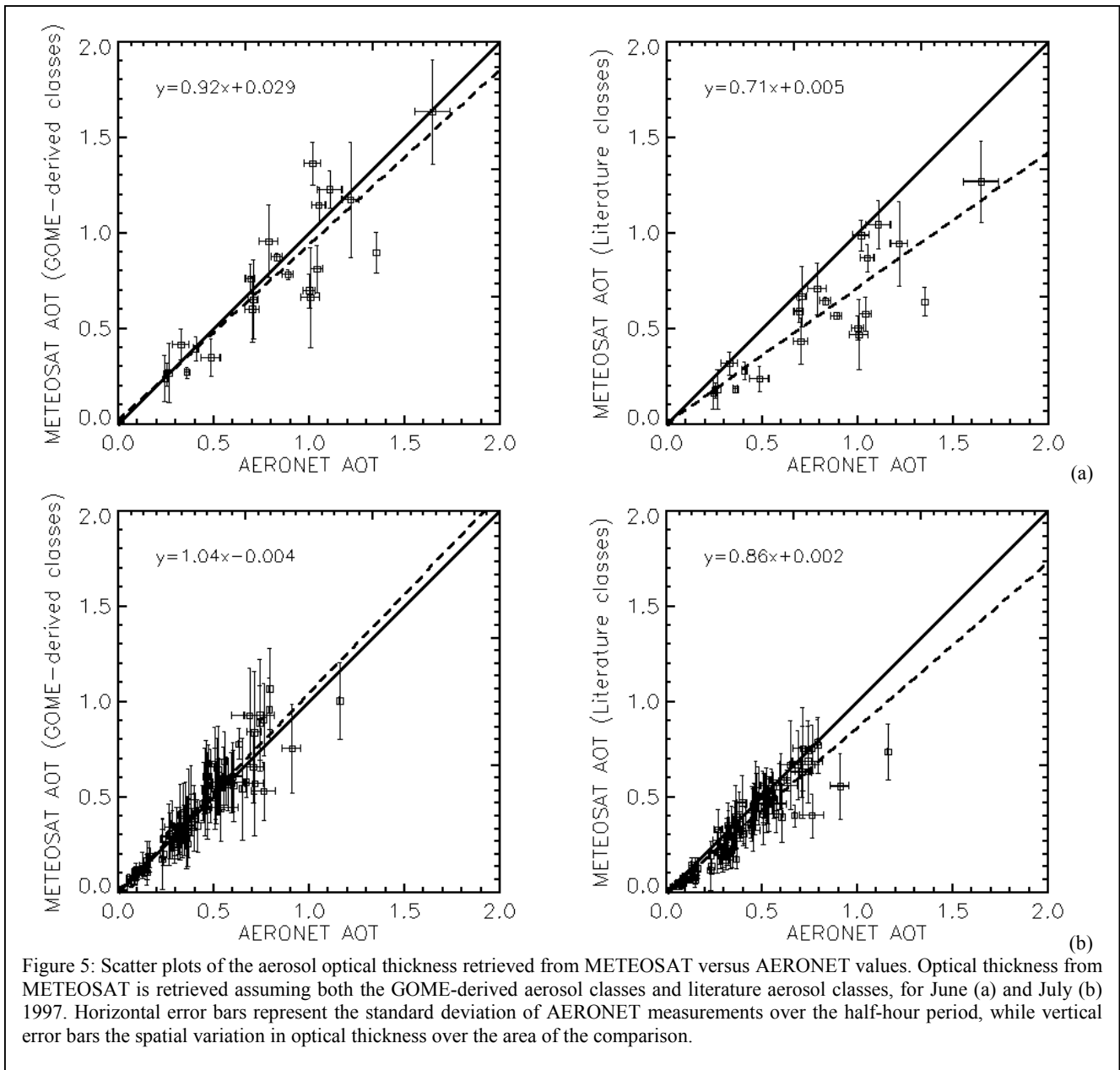


Figure 5 represents the scatter plots of the optical thickness retrieved from METEOSAT, using GOME-derived aerosol classes and literature aerosol classes, versus AERONET measurements, for June and July 1997, after the data screening. Horizontal error bars represent the standard deviation of AERONET measurements over the half-hour period. Vertical error bars reflect the spatial variation in optical thickness over the area taken for the comparison.

A larger number of comparison points are obtained for July, since all METEOSAT-6 slots have been processed. The same is being done for June, but work is still in progress. In general, there is a considerable agreement between optical thicknesses retrieved from METEOSAT using GOME-derived aerosol classes and measured values from AERONET. Some of the differences may be due to the larger spread of METEOSAT values in the averaged area. Nevertheless, even in these cases the agreement is better than for the literature aerosol classes, which seem to present a tendency to underestimate aerosol optical thickness values. Note that the agreement is quite well maintained in July although aerosol properties slightly changed. This can be due to the fact that the aerosol optical thickness values observed during the month of July are lower than those observed in June. Most of the values are lower than 0.8, whereas in June the aerosol optical thickness exceeds 1.0 for a number of cases. As already shown in Figure 2, the importance of the aerosol class increases with the optical thickness, therefore it is greater in June than in July. In fact, the disagreement between measurements and retrievals for the literature classes is lower in July, with a slope of 0.86, against 0.71 in June.

This shows that although METEOSAT has only a broadband channel in the visible spectral region, when its data are combined with the actual aerosol classes they can be used for aerosol studies significantly improving the accuracy with respect to the use of literature aerosol classes. This is especially true for situations of high aerosol loads, as stated by the comparisons with AERONET measurements.

Aerosol optical thickness retrieved from METEOSAT for June 1997 is also compared to the corresponding results derived from POLDER measurements. Coincident areas of $0.5^\circ \times 0.5^\circ$ are averaged and compared, for the best time coincidence (maximum 15 minute difference). The percentage of averaged pixels with respect to the total number of pixels in the area is calculated and the cell is retained for comparison only if this percentage exceeds 40%.

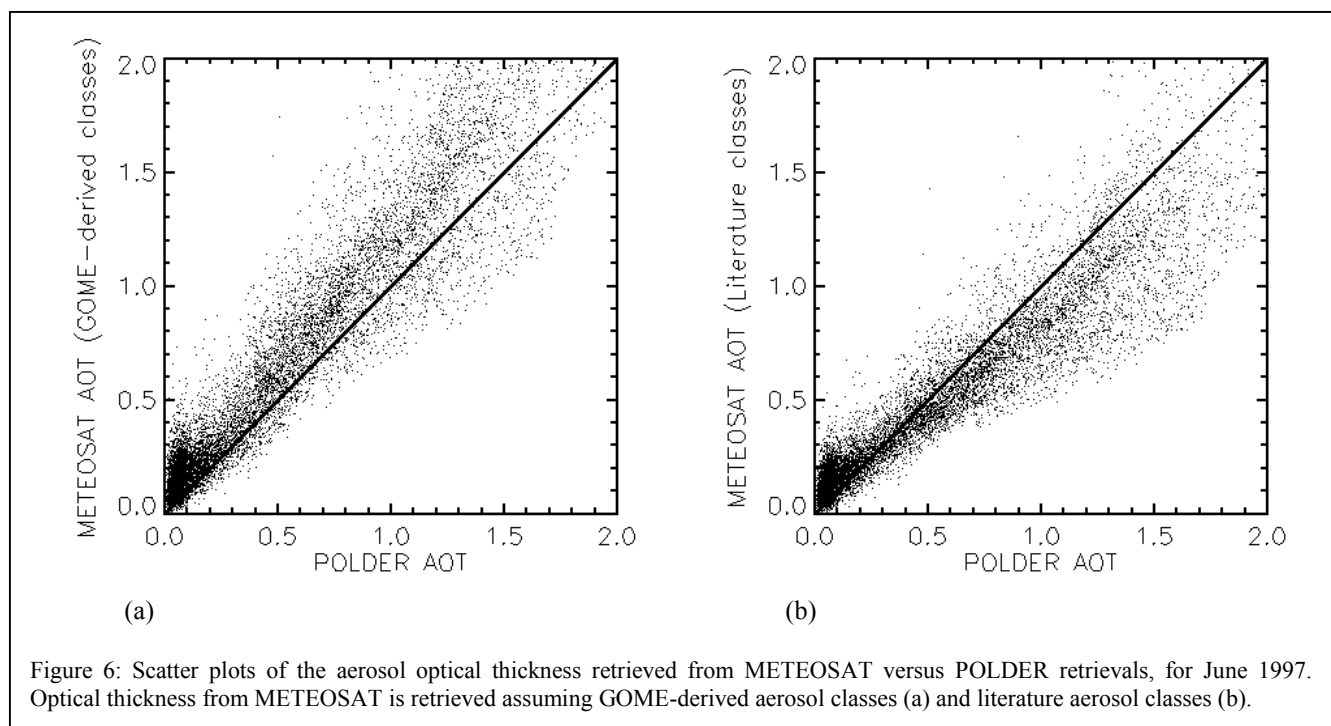


Figure 6: Scatter plots of the aerosol optical thickness retrieved from METEOSAT versus POLDER retrievals, for June 1997. Optical thickness from METEOSAT is retrieved assuming GOME-derived aerosol classes (a) and literature aerosol classes (b).

Figure 6 shows the scatter plots of METEOSAT versus POLDER aerosol optical thickness, respectively for the case of aerosol characterization with GOME-derived aerosol classes and literature classes. Results refer to the whole month of June 1997, within the limits of 10° - 30° N latitude and 10° - 50° W longitude. Data for July is not compared since the POLDER

instrument ceased operations at the end of June 1997. There is a growing dispersion of points as the optical thickness increases, which may be due to differences in the algorithms. On one hand, the LUTs built for the retrieval of the optical thickness from POLDER have 0.6 as the largest value⁹. This means that larger values are obtained by linear extrapolation, possibly leading to an under or overestimation of the values. The largest value shown in the graphs is 2.0, considered acceptable for the validation, since afterwards the dispersion becomes too large. On the other hand, aerosol absorption is taken into account in the present method, but not considered in POLDER algorithm. This may be the cause for the systematic differences observed in the plots. In order to compare results on the same basis, our values are homogenized to those of POLDER assuming a pure scattering approximation and thus multiplying the optical thickness by the single scattering albedo at 0.55 μm . The value obtained from Mie calculations for the single scattering albedo for the GOME-derived desert aerosol class is 0.90 and for the literature desert class 0.93. These results are illustrated in the scatter plots of Figure 7. After homogenizing aerosol optical thickness values to those of POLDER a clear approximation arises for both of them when using GOME-derived aerosol classes. As for the literature classes, once more a trend is observed that indicates an underestimation of the optical thickness.

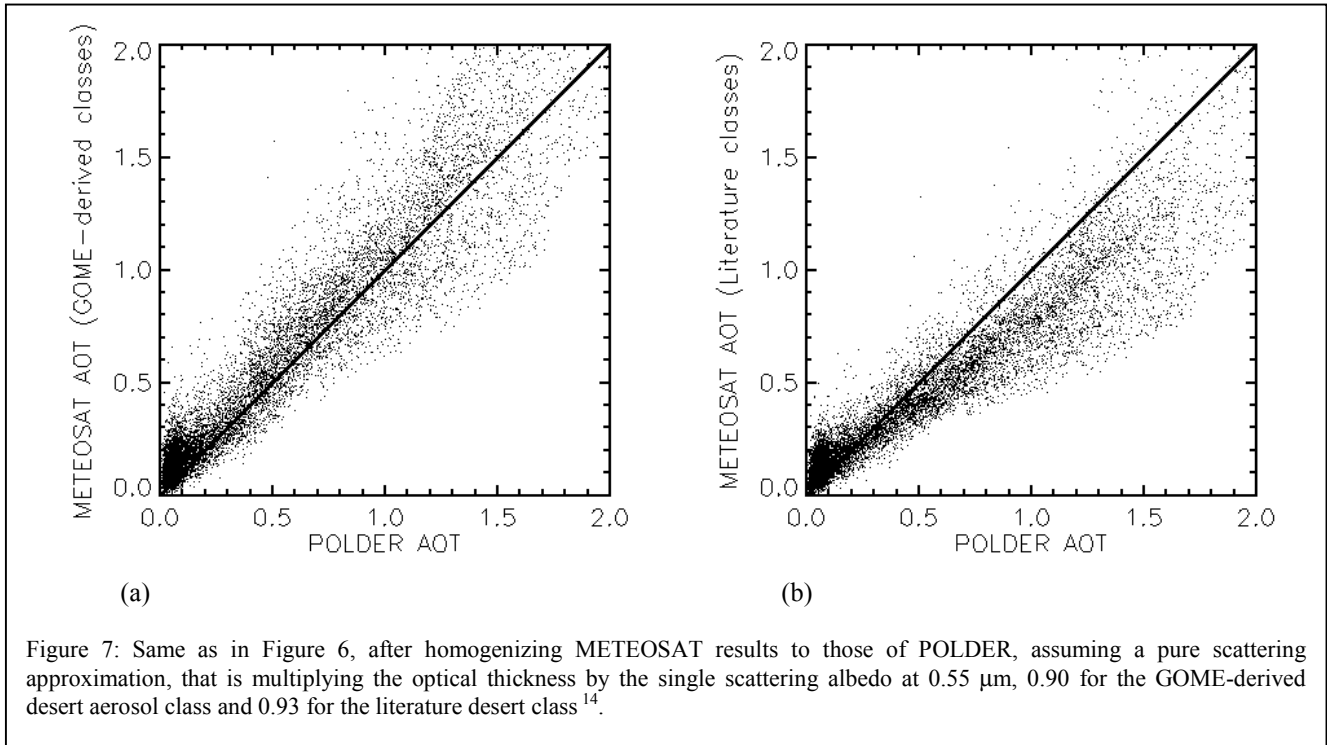


Figure 7: Same as in Figure 6, after homogenizing METEOSAT results to those of POLDER, assuming a pure scattering approximation, that is multiplying the optical thickness by the single scattering albedo at 0.55 μm , 0.90 for the GOME-derived desert aerosol class and 0.93 for the literature desert class¹⁴.

The problem of selecting the adequate aerosol class for each pixel is addressed using the bi-spectral METEOSAT classification, which attributes a class to each pixel. According to this classification, the maritime or the desert type classes are used. The spatial validity of the retrieved aerosol classes is taken into account, applying the method only over the area where the class is retrieved without extending it to different geographical locations, where new classes should be derived corresponding to different aerosol events.

As for the temporal limit of effectiveness of the aerosol class derived, it requires further investigation with longer temporal series of data, an investigation the authors intend to carry on in the near future. Nevertheless, for the cases presented in this work, it seems that the effectiveness of the class is maintained at least for the whole month of June 1997.

4. CONCLUSIONS

The proposed method is a powerful tool for aerosol characterization and optical thickness monitoring over the oceanic areas covered by geostationary satellites, especially for strong aerosol events as the case studies presented. High latitude regions are well covered by polar orbiting satellites that can be conveniently used. Results show that the choice of the aerosol class

is crucial for accurate retrievals; consequently atmospheric aerosol characterization should as much as possible be representative of the real situation.

The comparison of the aerosol optical thickness retrieved from METEOSAT with independent measurements from AERONET reveals a good agreement when GOME-derived aerosol classes representative of the actual aerosol situation are used. The same can be concluded from comparisons with aerosol optical thickness results obtained from POLDER data. This is a clear indication that the aerosol classes derived from GOME spectral measurement fitting better represent the real aerosol conditions, at least over a limited area and time period. Further investigation is needed to establish these limits.

New sensors like SEVIRI (Spinning Enhanced Visible and InfraRed Imager) that will fly onboard the METEOSAT Second Generation (MSG) and AATSR, MERIS and SCIAMACHY onboard the soon to be launched polar orbiting ENVISAT-1, are expected to bring improvements to the present algorithm. On one hand, the better calibration and spectral response accuracy as well as the narrower visible and the new near infrared spectral bands that SEVIRI will provide allow for more accurate aerosol characterization. On the other hand the synergistic use of the three nadir viewing spectrometers in ENVISAT-1 will enlarge the present spectral coverage and provide better spatial resolution with respect to GOME's, thus contributing to improve the detection and characterization of atmospheric aerosols^{17, 18}.

ACKNOWLEDGEMENTS

METEOSAT imagery was kindly made available by EUMETSAT. The work was supported by Agenzia Spaziale Italiana (ASI) through contract *Sinergia GERB-SEVIRI nello Studio del Bilancio Radiativo a Scala Regionale e Locale* and European Space Agency (ESA-ESRIN) through contract *Improvement and Validation of the GASP Aerosol Product*. AERONET data are available at <http://aeronet.gsfc.nasa.gov:8080/> thanks to NASA, CNES and CNRS. POLDER aerosol parameters presented in this paper were obtained using data from CNES's POLDER onboard NASDA's ADEOS. MJC was financially supported by the *Subprograma Ciência e Tecnologia do 2º Quadro Comunitário de Apoio*.

REFERENCES

1. Costa, M. J., M. Cervino, E. Cattani, F. Torricella, V. Levizzani, and A. M. Silva, "Aerosol optical thickness and classification: use of METEOSAT, GOME, and modelled data", *Proc. SPIE: Satellite Remote Sensing of Clouds and the Atmosphere IV*, J. E. Russell Ed., vol. 3867, pp. 268-279, Firenze, 1999.
2. Rosenfeld, D., "Suppression of rain and snow by urban and industrial air pollution", *Science*, vol. 287, pp. 1793-1796, 2000.
3. Rosenfeld, D., "TRMM observed first direct evidence of smoke from forest fires inhibiting rainfall", *Geophys. Res. Lett.*, vol. 26, pp. 3105-3108, 1999.
4. Moulin, C., F. Guillard, F. Dulac, and C. E. Lambert, "Long-term daily monitoring of Saharan dust load over ocean using METEOSAT ISCCP-B2 data: 1. Methodology and preliminary results for 1983-1994 in the Mediterranean", *J. Geophys. Res.*, vol. 102, pp 16,947-16,958, 1997.
5. Griggs, M. "Satellite observations of atmospheric aerosols during the EOMET cruise", *J. Atmos. Sci.*, vol. 36, pp. 695-698, 1979.
6. Burrows, J. P. , M. Weber, M. Buchwitz, V. Rozanov, A. Ladstätter-Weißmeyer, A. Richter, R. DeBeek, R. Hoogen, K. Bramstedt, K.-U. Eichmann, and M. Eisinger, "The Global Ozone Monitoring Experiment (GOME): Mission concept and first scientific results", *J. Atmos. Sci.*, vol. 56, pp. 151-175, 1999.
7. Bartoloni, A., P. Colandrea, R. Loizzo, M. Mochi, F. Pascuali, N. Santantonio, E. Zappitelli, and M. Cervino, "SYSGOME: Processing chain for aerosol optical thickness product generation at I-PAF", *Proc. 2000 EUMETSAT Meteorological Satellite Data Users' Conf.*, pp. 460-467, Bologna, 2000.
8. Torricella, F., E. Cattani, M. Cervino, R. Guzzi, and C. Levoni, "Retrieval of aerosol properties over the ocean using GOME measurements: Method and applications to test cases", *J. Geophys. Res.*, vol. 104, pp 12,085-12,098, 1999.
9. Goloub, P., D. Tanré, J.L. Deuzé, M. Herman, A. Marchand, and F-M. Bréon, "Validation of the first algorithm for deriving the aerosol properties over the ocean using the POLDER/ADEOS measurements", *IEEE Trans. Geosci. Remote Sensing*, vol. 37, pp. 1586-1596, 1999.

10. Porcú, F., and V. Levizzani, "Cloud classification using METEOSAT VIS-IR imagery", *Int. J. Remote Sensing*, **vol. 13**, pp 893-909, 1992.
11. Vermote, E. F., D. Tanré, J.-L. Deuze, M. Herman, and J.-J. Morcrette, "Second simulation of the satellite signal in the solar spectrum: An overview", *IEEE Trans. Geosci. Remote Sensing*, **vol. 35**, pp. 675-686, 1997.
12. Costa, M. J., M. Cervino, E. Cattani, F. Torricella, V. Levizzani, and A. M. Silva, "An update of a GOME-METEOSAT method for aerosol optical thickness determination and classification", *Proc. 2000 EUMETSAT Meteorological Satellite Data Users' Conf.*, pp. 420-427, Bologna, 2000.
13. Press, W. H., S. A. Teukolsky, W. T. Vetterling, and B. P. Flannery, *Numerical Recipes in Fortran 77*, 2nd ed., vol. 1, pp. 436-448, Cambridge University Press, Cambridge, 1997.
14. Shettle, E. P., "Optical and radiative properties of a desert aerosol model", *International Radiation Symposium (IRS): Current problems in atmospheric radiation*, G. Fiocco Ed., pp. 74-77, A. Deepak, Hampton, Va., 1984.
15. Dubovik, O., and M. King, "A flexible inversion algorithm for retrieval of aerosol optical properties from sun and sky radiance measurements", *J. Geophys. Res.*, **vol. 105**, pp 20,673-20,696, 2000.
16. Dubovik, O., A. Smirnov, B. Holben, M. King, Y. Kaufman, T. Eck, and I. Slutsker, "Accuracy assessments of aerosol optical properties retrieved from Aerosol Robotic Network (AERONET) Sun and sky radiance measurements", *J. Geophys. Res.*, **vol. 105**, pp 9791-9806, 2000.
17. Torricella, F., E. Cattani, M. Cervino, V. Levizzani, and M. J. Costa, "Simulations of time-coincident, co-located measurements from ENVISAT-1 instruments for the characterization of tropospheric aerosol: a sensitivity study including cloud contamination effects" *Atmos. Sci. Lett.*, **vol 1**, doi:10.1006/asle.2000.0021, <http://www.academicpress.com/asl>, 2000.
18. Cervino, M., E. Cattani, F. Torricella, M. Mochi, D. Cerchia, P. Colandrea, M. Silvestri, and L. De Fusco, "Synergistic use of MERIS and SCIAMACHY instruments on board of ENVISAT-1: a test case with simulated data", *Proc. 2000 EUMETSAT Meteorological Satellite Data Users' Conf.*, pp. 436-442, Bologna, 2000.